Nanostructured modified electrodes: Role of ions and solvent flux in redox active polyelectrolyte multilayer films†

Mario Tagliazucchi, Doris Grumelli‡ and Ernesto J. Calvo*

Received 30th June 2006, Accepted 14th August 2006
First published as an Advance Article on the web 24th August 2006
DOI: 10.1039/b609341h

Electrodes modified layer-by-layer by self-assembly of redox active polyelectrolytes comprised of osmium bipyridine–pyridine derivatized poly(allyl-amine) and poly(vinyl) sulfonate have been studied by EQCM, ellipsometry, cyclic voltammetry and electrochemical impedance spectroscopy in aqueous solutions of different anions and cations. Redox driven swelling by solvent exchange during oxidation, in excess to the hydration number, occurs by perturbation of the equilibrium between the osmotic and elastic forces as a result of the electrochemical injection of charge into the film. The exchanged mass and volume change during redox switching strongly depends on the nature of the anion under anion Donnan permselectivity conditions.

Introduction

Layer-by-layer self assembly of redox polyelectrolytes allows the fabrication of electroactive nanometer thin films on electrode surfaces with a fine tuning of film thickness and a precise spatial organization. The choice of adsorption pH,[1] salt concentration[2–4] and the nature of polyelectrolytes has dramatic consequences on the multilayer structure, while the ion-exchange[5] and the electrochemical response[6] are also affected by the excess charge in the topmost layer. The ability to control polyelectrolyte multilayer (PEM) structure and functionality, in addition to its high reproducibility and low cost, make the LbL technique an attractive option as compared to conventional preparation methods of polymer modified electrodes such as electropolymerization, spin coating or film casting. Thus, it is not surprising that several examples of PEM modified electrodes have been reported: polyviologen[7,8] for electrochromic and electrocatalytic devices, poly(allyl-amine) with covalently attached ferrocene (PAH-Fc)[9] or osmium bipyridil (PAH-Os)[10–12] and glucose oxidase (GOx) assemblies for glucose biosensors, polyoxometallates for electrocatalysis,[13] sulfonated polyaniline (SPAN) and cytochrome C multilayers for peroxide determination,[14] water-soluble poly(*p*-phenylene) for LED fabrication,[15] *etc*.

Electrostatically self-assembled polyelectrolyte films are highly sensitive to their environment. For example, Schlenoff has shown that when a PEM is transferred to a salt solution the polyelectrolyte–polyelectrolyte (intrinsic) charge compensation in the multilayer evolves to an extrinsic charge compensation due to the incorporation of mobile ions in the film, producing swelling and smoothing,[16] improved permeability [17,18] and polyelectrolyte interdiffusion.[19] The pH of the outer solution also affects the PEM when at least one of the components is a weak polyelectrolyte; for example Rubner has demonstrated that low pH treatment could lead to abrupt swelling transitions[20,21] and pH-induced microporosity.[21] The effect of the solution electrolyte on the structure and electro-chemical response of redox PEMs has been studied to a much lesser extent.

In the present work, we have analyzed the influence of different electrolyte compositions in the electrochemistry of PAH-Os/PVS films, considering not only the charge transport but also the electrochemically driven fluxes of ions and solvent. During the last decade, similar studies have been carried out with a variety of chemically modified electrodes such as electropolymerized,[22,23] cast[24] or electroprecipited[25,26] polymer modified electrodes.

Some salient features of PEM modified electrodes redox behavior have been obtained for the system PAH-Os (self-assembled at pH 8.3)/PVS and should be considered to have a complete picture of the electrochemical processes:

1. The electrochemistry is highly dependent on the nature of charge in the topmost layer.[6] For positively capped multilayers, the charge transport inside the film can be described employing a bound diffusion model.[6,27]

2. The amount of net fixed charges in the film, calculated from the Donnan *E vs.* log *c* plot, is positive.[28] This means that the film is an anion exchanger, provided that the electrolyte concentration is below the Donnan breakdown concentration, *ca.* 0.5 M.

3. Probe beam deflection technique (PBD) has confirmed that the anions are the most important contribution (even for negatively capped films) to maintain film electroneutrality during redox switching.[5,29]

4. Fourier transform infrared spectroscopy (FTIR) has shown that during oxidation the film uptakes water and releases it during reduction of Os(III).[27]

5. During oxidation–reduction cycles, swelling–de-swelling of the film has been observed by *in situ* ellipsometry.[12,27]

INQUIMAE, Departamento de Química Inorgánica, Analítica y Química Física, Facultad de Ciencias Exactas y Naturales, Universidad de Buenos Aires, Buenos Aires, C1428EHA, Argentina
† Electronic supplementary information (ESI) available: Ψ *vs.* Δ plot (Fig. 1S) and ellipsometric thickness (Fig. 2S) for the assembly of PAH-Os/PSS multilayer. See DOI: 10.1039/b609341h.
‡ Present Address: INIFTA, cc. 16, suc 4, 1900 La Plata, Argentina, E-mail: dgrumell@qi.fcen.uba.ar.

In the present paper we have chosen to employ different and complementary techniques (cyclic voltammetry, EIS, EQCM and ellipsometry) in order to systematically study the redox swelling and charge transport in multilayer films in contact with electrolyte solutions of different cations (NaCl, CsCl, LiCl, HCl) and anions (NaCl, NaF, $NaNO_3$, $NaBF_4$, $NaClO_4$).

The paper describes the results of the different experimental techniques and discusses the forces involved in the electrochemically driven swelling and ionic exchange between the film and the electrolyte.

2. Experimental

2.1. Reagents and materials

All solutions were prepared with 18 MΩ Milli-Q® (Millipore) water. The following chemicals were used without further purification: poly(sodium 4-styrenesulfonate), PSS (MW ~ 70 000, Aldrich); Poly(sodium vinyl-sulfonate), PVS (25 wt% solution in water, Aldrich); sodium 3-mecapto-propane-sulfonate, MPS (Aldrich). Salts employed in electrolyte solutions (NaCl, NaF, $NaNO_3$, $NaClO_4$, $NaBF_4$, CsCl, LiCl) and HCl were of analytical grade and used as received.

The osmium bipyridine derivatized redox polymer Os $(bpy)_2ClPyCH_2NH$-poly(allylamine), PAH-Os, was synthesized as previously reported.[30] Thiol solutions of 20 mM 3-mercapto-1-propane-sulfonic acid (MPS) (Aldrich) in 10 mM sulfuric acid (Merck) were prepared before each experiment in order to avoid oxidation in air. No salt was added to polyelectrolyte solutions, however their pH was adjusted to 8.3. Under these conditions only 60–70% of the primary amine groups in PAH-Os are protonated,[31] producing thick films due to the low charge density of the PAH-Os chains.[1]

2.2. Surface modification

Silicon (100) substrates were coated with a 20 nm titanium and 20 nm palladium adhesion layer and a 200 nm gold layer, thermally evaporated with an Edwards Auto 306 vacuum coating system at $P < 1.10^{-8}$ bar, and employed as electrodes.

Alternatively, 10 MHz Au-coated 14 mm in diameter and 0.168 mm in thickness AT-cut quartz crystals with an active area of 0.196 cm^2 (International Crystal Manufacturing Company Inc., Oklahoma City, cat.no.31210) were employed for EQCM measurements.

In the first step, the gold film substrates were primed with sulfonate groups by immersion in an MPS solution for 30 min, followed by rinsing with deionized water. After thiol adsorption, the first polycation layer was deposited on thiol-modified Au substrate by immersion in PAH-Os (pH = 8.3) solution for 15 min, followed by thoroughly rinsing with Milli-Q water. The next and subsequent layers were deposited onto the modified surface by alternate immersion in a solution of the respective polyanion (PVS or PSS) or polycation (PAH-Os) for 15 min and rinsing with Milli-Q water until the desired number of layers was achieved. The adsorption times were previously determined by ellipsometric transient measurements and EQCM.[32]

2.3. Electrochemical experiments

Electrochemical measurements were carried out at room temperature (20 ± 2 °C) with an Autolab PGSTAT 30 potentiostat (Autolab, Ecochemie, Holland) equipped with a FRA2 frequency response analyzer module for impedance measurements. All experiments were performed in a purpose built three electrode Teflon cell, with an electrode exposed area of approximately 0.25 cm^2 delimited by an inert 'o'-ring.

For reference electrode, Ag/AgCl; 3 M KCl was employed and all electrode potentials herein are referred to it; a platinum gauze auxiliary electrode of large area was employed. Before thiol adsorption the electrode potential was cycled in 2 M sulfuric acid between 0.2 and 1.6 V at 0.1 V s^{-1} to check for surface contamination and electrochemically active areas were calculated from the reduction peak of gold oxide.[33]

Electrochemical impedance spectra were acquired in the frequency range from 25 kHz to 50 mHz with a 10 mV amplitude of oscillation. Data analysis and fitting were performed with the program ZView® (Scribner Associates, USA).

2.4. Electrochemical quartz crystal microbalance

The quartz crystal resonator at 10 MHz was used as a quartz crystal microbalance (QCM) with a complex voltage divider to measure the resonant frequency and both components of the quartz crystal Butterworth-Van Dyke equivalent circuit, which has been described elsewhere.[34] The crystals were mounted in the cells by means of Viton© O-ring seals, with only one face in contact with the electrolyte; this electrode was a common ground to both the ac and dc circuits. Previous results for the system PAH-Os/PVS have shown that this film could be considered as acoustically thin[35] and therefore frequency shifts have been directly transformed into mass changes employing the Sauerbrey equation.

2.5. Ellipsometry

For ellipsometric measurements a Sentech variable angle rotating-analyzer automatic ellipsometer (vertical type, 2000 FT model) equipped with a 632.8 nm laser as polarized light source was employed. All measurements were performed at an incidence angle of 70.00°. The gold coated silicon electrode was horizontally mounted in Sentech liquid cell (E-SE400-20) fitted with two glass optical windows (positioned for 70.00° with an accuracy of 0.01°). All adsorption steps were carried out avoiding any variations of the electrode position in order to keep the system alignment. Ellipsometric parameter variations lower than the data dispersion for a single measurement (0.01 in ψ and 0.05 in Δ) were guaranteed in this way.

Ellipsometric angles ψ and Δ were determined from reflection-induced changes in the state of polarization of linearly polarized light, these were related to the ellipsometric ratio ρ:

$$\rho = \tan(\psi)\exp(i\Delta) = \frac{r_p}{r_s} \qquad (1)$$

where tan ψ represents the amplitude change in ρ, Δ is the phase difference change, and r_p and r_s are the complex reflection coefficients for light polarized parallel and perpendicular to the plane of incidence which depend on the structure and optical properties of the system.

Ellipsometric parameters, ψ and Δ, were collected manually after each adsorption step or continuously during potential sweep or chronoamperometric transients with the modified electrode surface in contact with the electrolyte solution. The experimental data were fitted as described elsewhere.[36] The fitting of ellipsometric parameter for *in situ* electrochemical experiments allows the determination of only two optical film parameters (absorption coefficient, refractive index or film thickness) and therefore the assumption that the absorption coefficient is equal to zero at the working wavelength was used.

Results

3.1. Electrochemistry

The first step to understand the importance of anions and cations in redox induced swelling of PAH-Os multilayers consists in the analysis of how the different electrolytes modify the electrochemical response. Fig. 1 depicts cyclic voltamperograms for a $(PAH\text{-}Os)_4(PVS)_4(PAH\text{-}Os)$ electrode in 10 mM solutions of NaCl and $NaClO_4$, respectively. All other electrolytes used in this work produce similar voltamperogram shapes to that obtained for NaCl. Peak parameters for all solutions employed are compiled in Table 1. It is worthwhile noting that the capping layer during this work was chosen to be always PAH-Os since polyanion capped films present a hindrance to redox switching as reported before.[6]

The cyclic voltammetry recorded using NaCl presents an almost reversible surface wave shape, with a peak separation of a few milivolts (probably due to ohmic drop by uncompensated solution resistance) and a full width at half height (FWHH) of nearly 90 mV. The peak current follows a linear relationship with the sweep rate (inset in Fig. 1) as expected for a Nernstian system.[37] For $NaClO_4$ electrolyte, a larger peak separation and a smaller redox charge become apparent and the voltamperogram presents a characteristic diffusion tail[38] while the current–sweep rate relationship is no longer linear (the current scales with $v^{0.88}$, where v is the sweep rate). The

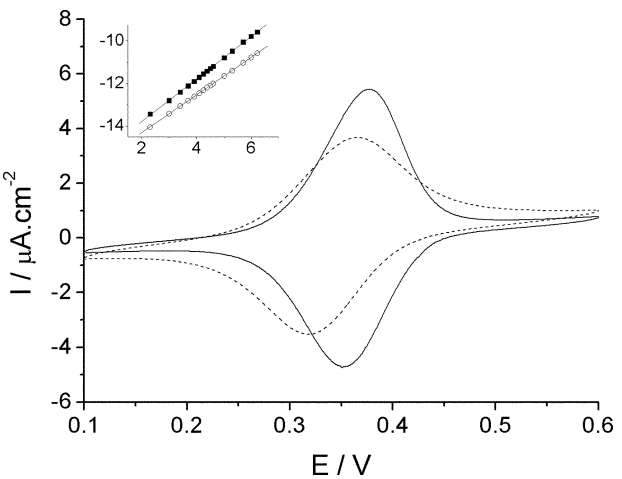

Fig. 1 Cyclic voltamperograms for $(PAH\text{-}Os)_5(PVS)_4$ electrode in NaCl 10 mM (solid line) and $NaClO_4$ 10 mM (dashed line). Scan rate: 25 mV s^{-1}. Inset: logarithm of peak current *versus* logarithm of velocity. Slopes of best linear fit are (0.997 ± 0.005) for NaCl (black squares) and (0.883 ± 0.002) for $NaClO_4$ (open circles).

Table 1 Peak parameters for cyclic voltamperograms of $(PAH\text{-}Os_5)/(PVS_4)$ electrode in 10 mM solutions of different 1 : 1 electrolytes. The same electrode was used for all experiments. Scan rate: 25 mV s^{-1}

Electrolyte	Q_{ox}/μC cm^{-2}	$E_{1/2}$/V	$(E_p^{ox} - E_p^{red})$/V
NaCl	19.2	0.365	0.027
NaF	20.7	0.374	0.036
$NaNO_3$	21.1	0.359	0.025
$NaBF_4$	18.9	0.378	0.031
$NaClO_4$	17.5	0.343	0.041
CsCl	18.7	0.364	0.025
LiCl	19.8	0.369	0.028
HCl[a]	17.2	0.394	0.034

[a] HCl was the measured at the end since irreversible charge losses where observed for this electrolyte.

effect of the perchlorate anion is totally reversible and the thin film voltammetry is recovered when the electrode is transferred back to a NaCl solution. If a mixed solution (5 mM Cl^- and 5 mM ClO_4^-) is employed, the voltamperogram is similar to that obtained in pure 10 mM $NaClO_4$, demonstrating that the electrochemistry is affected by the presence of perchlorate and not by the lack of chloride.

In addition to $NaClO_4$, the other electrolyte that produces significant changes in peak parameters is HCl. For this electrolyte, the average peak potential is shifted to higher values, which could be explained as a shift in the Donnan potential due to protonation of free amino groups at lower pH.[39] Table 1 also reveals that HCl gives raise to the smallest redox charge. However, this effect was observed to be irreversible and probably due to structural changes in the protonated film.[20,21] Thus experiments in HCl were always performed at the end.

To further characterize the effect of ClO_4^- in the electron transport, we have employed electrochemical impedance spectroscopy (EIS). Fig. 2 shows the Bode plots ($\log|Z|$ *vs.* $\log f$ and θ *vs.* $\log f$ plots)[40] for a $(PAH\text{-}Os)_4(PVS)_4(PAH\text{-}Os)$ electrode in 100 mM NaCl and $NaClO_4$. These spectra were acquired at the apparent $E^0_{Os(III)/Os(II)}$, which was previously determined by cyclic voltammetry for each electrolyte. A complete discussion of the impedance spectrum features of PAH-Os/PVS films has been published elsewhere.[6] A simple analysis shows that in the whole frequency range investigated the impedance increases when chloride is replaced by perchlorate.

A more detailed analysis requires fitting the whole EI spectra employing an appropriate equivalent circuit. The modified Randles circuit[41] shown in the inset of Fig. 2A has the advantage of being simple and all of its components having a physical representation. It consists of the uncompensated ohmic electrolyte resistance, Rs in series with an impedance given by the double layer capacitance, C_{DL} in parallel with the charge transfer resistance R_{CT} and a finite diffusion or bound diffusion impedance, Z_D.

The latter is given by:[42]

$$Z_D(\omega) = \left[\exp\left(\frac{\eta F}{2RT}\right) + \exp\left(-\frac{\eta F}{2RT}\right)\right]^2 \frac{RT}{F^2\Gamma_{Os}} \times \frac{1}{(jD_{app}\omega)^{1/2}} \coth\left[d\left(\frac{j\omega}{D_{app}}\right)^{1/2}\right] \quad (2)$$

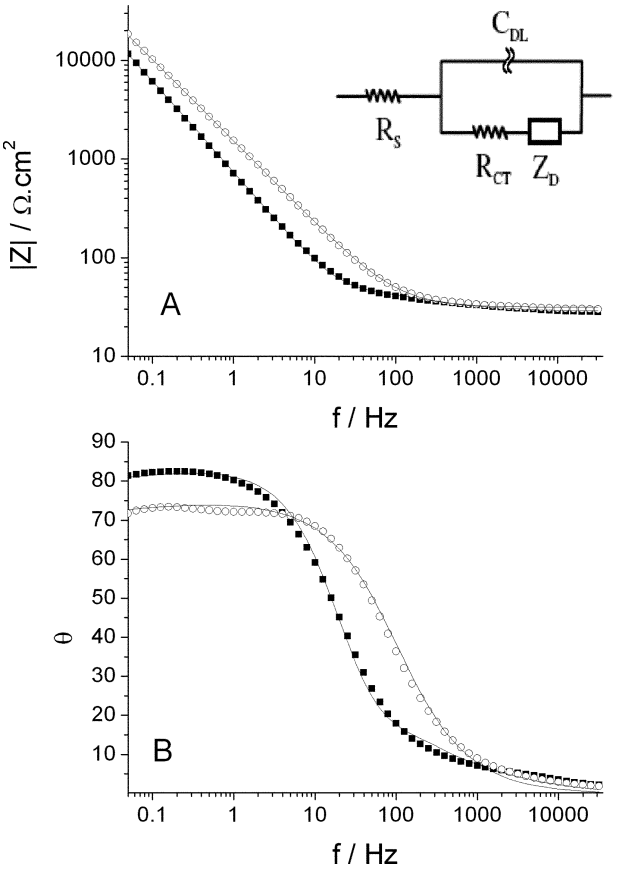

Fig. 2 (A) $|Z|$ *vs.* f and (B) θ *vs.* f plots (Bode plots) for a (PAH-Os)$_5$(PVS)$_4$ electrode in NaCl 100 mM (solid squares) and $NaClO_4$ 100 mM (open circles). Solid lines are the best fits to the equivalent circuit shown as an inset. See Table 2 for fitting parameters.

where ω is the angular frequency, η is the electrode apparent overpotential: $E - E^{0\prime}_{Os(III)/OS(II)}$, D_{app} is the apparent electron diffusion coefficient and Γ_{Os} is the surface concentration of electrochemically accessible osmium sites. The impedance Z_D behaves as a Warburg impedance at high frequencies (describing charge transport inside the film) and as a capacitor at low frequencies since the maximum redox capacitance is limited by the amount of osmium sites available in the film.

To account for frequency dispersion due to film roughness, the double layer capacitance is modeled using a constant phase element (CPE)[43] rather than an ideal capacitor:

$$Z_{CPE} = \frac{1}{C}\left(\frac{1}{i\omega}\right)^n \qquad (3)$$

where n is the CPE phase and C is a constant with units F s^{n-1}

It should be noticed that, except for the simplest equivalent circuits, several sets of parameters can be accurately fitted to a given EI spectra. Thus the determination of a set of parameters (local minima in the sum of squared residuals) is highly dependant on the seed values employed. In the present study, we have first performed the fitting for the experiment with NaCl, using as seed parameters those previously obtained for PAH-Os/PVS.[6,27] We then employed the resulting parameters as seed values to fit the spectrum recorded in $NaClO_4$, setting the restriction that the osmium surface coverage must be equal to that obtained in NaCl (the same electrode was used in both experiments). The fit solution was finally minimized with respect to all the parameters. Table 2 contains the fitting parameters and the simulated curves are plotted in Fig. 2 for comparison.

Table 2 Fitting parameters obtained from the electrochemical impedance spectra of a (PAH-Os)$_5$(PVS)$_4$ electrode (see Fig. 2) in 100 mM electrolyte solutions

	NaCl	$NaClO_4$
$Q/\mu C\ cm^{-2}$	14.7	14.6
$D_{app}/cm^2\ s^{-1}$	1.8×10^{-10}	6.6×10^{-15}
$R_{CT}/\Omega\ cm^2$	4.9	165
$R_S/\Omega\ cm^2$	28.8	31.4
$C_{DL}/F\ s^{n-1}\ cm^{-2}$	1.12×10^{-4}	1.34×10^{-4}
n (C_{DL})	0.79	0.84

Q: osmium redox charges in the film; D_{app}: Apparent electron diffusion coeficient; R_{TC}: charge transfer resistance; C_{DL}: value for double layer capacitance modelled as a CPE with phase equal to n.

Inspection of Table 2 reveals that the presence of perchlorate produces a drastic decrease of nearly five orders of magnitude in the apparent electron diffusion coefficient, as well as a considerable increase in the charge transfer resistance.

3.2 Electrochemical quartz crystal gravimetry

Fig. 3 and 4 show the evolution of areal mass (A) and charge density (B) transients for a (PAH-Os)$_{14}$(PVS)$_{14}$PAH-Os film in 10 mM sodium electrolyte solutions of different anions and 10 mM chloride electrolyte solutions of different cations, respectively, during the oxidation and reduction of the osmium in the film. In these experiments, the electrode was first pre-treated at 0.1 V for 120 s to ensure complete reduction of the redox sites and a potential step to 0.6 V was applied recording both mass and current transients simultaneously for 60 s of oxidation, followed by a potential step to 0.1 V, where reduction of Os(III) takes place.

Every few experiments, a measurement in NaCl was performed. Good reproducibility in these control experiments was obtained, which assured the integrity of the LbL film electrodes and the reproducibility of the data.

Mass changes during the redox process for a (PAH-Os)$_{14}$(PVS or PSS)$_{14}$PAH-Os electrode have previously been discussed:[27] mass increases during oxidation and decreases during reduction.

The increase in mass upon oxidation in Fig. 3 is very dependent on the anion of the bathing solution: Cl^- and F^- yield the highest exchanged masses and ClO_4^- the lowest. On the other hand, mass and charge transients for chloride solutions with different cations (Fig. 4) do not differ appreciably from those recorded in NaCl solution beyond the differences in control experiments.

The Faradaic current also depends on the anion employed consistently with cyclic voltammetry experiments: Cl^-, F^-, and NO_3^- yield approximately the same redox charge, a smaller charge is obtained for BF_4^-, while ClO_4^- yields even

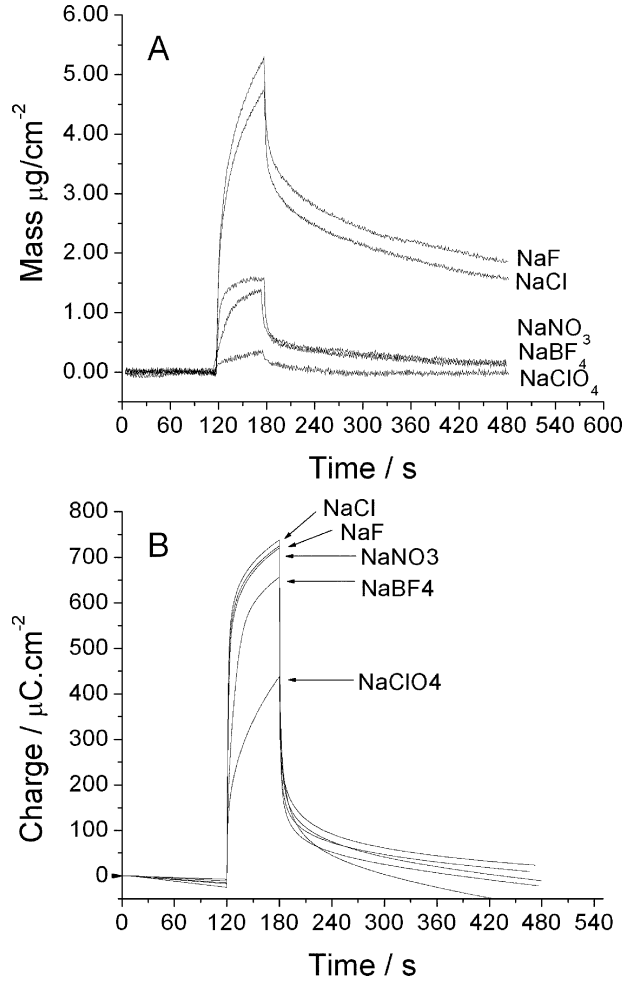

Fig. 3 Mass (A) and charge (B) transients for the redox switching of a $(PAH\text{-}Os)_{15}(PVS)_{14}$ film in different sodium 10 mM electrolyte solutions. The electrode potential was kept at 0.1 V for 120 s, followed by a step to 0.6 V. This potential was maintained for 60 s before a step back to 0.1 V.

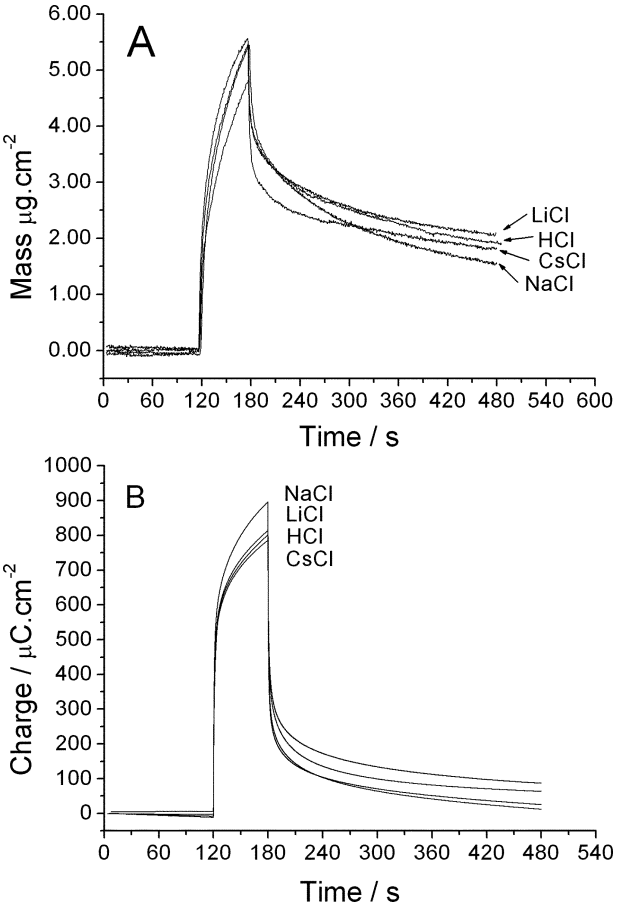

Fig. 4 Mass (A) and charge (B) transients for the redox switching of a $(PAH\text{-}Os)_{15}(PVS)_{14}$ film in different chloride 10 mM electrolyte solutions. See caption in Fig. 3 for the potential program applied.

a smaller charge. Since both mass and charge transients depend on the anion, the exchanged molar mass has been normalized per mole of electrons.

Fig. 5 shows mass to charge plots for the transients depicted in Fig. 3 and 4. The hysteresis in the oxidation/reduction transients show that the solvent exchange is delayed with respect to injection of charge. Hillman reported similar effects of different timescales for solvent and anions for poly(vinylferrocene).[44,45] In PAH/PVS films the hysteresis decreases after repetitive redox cycling as previously reported.[27] We have therefore chosen to use only the first redox cycle for each electrolyte in order to avoid irreversible charge loss or morphological changes in the PEMs during the complete set of experiments.

The mass-to-charge curves show a strong dependence of the exchanged mass with the nature of the electrolyte (Fig. 5A). On the other hand, the end-to-end exchanged molar masses (see Table 3) confirm that the difference observed for different cations is within the experimental error.

3.3 Ellipsometry

The combination of *in situ* ellipsometry with electrochemical methods allows the direct determination of film thickness as a function of the oxidation state of the redox polyelectrolyte multilayer. Fig. 6 depicts film thickness and refractive index obtained for a $(PAH\text{-}Os)_{14}(PSS)_{14}PAH\text{-}Os$ electrode during

Table 3 End to end mass to charge relationships for data in Fig. 3 and 4

Sodium salts	$(\Delta m/\Delta q)$ [a]/ g C^{-1} ($\times 10^3$)	Δm [a]/ g mol^{-1} ($\times 10^3$)	N_{H_2O}
NaCl	64 ± 9	615 ± 90	32
NaF	72 ± 9	692 ± 90	37
$NaNO_3$	19 ± 9	185 ± 90	7
$NaBF_4$	20 ± 9	195 ± 90	6
$NaClO_4$	6 ± 9	58 ± 90	−2.3
Chloride salts			
NaCl	62 ± 9	598 ± 90	31
LiCl	62 ± 9	596 ± 90	31
CsCl	58 ± 9	564 ± 90	29
HCl	69 ± 9	662 ± 90	35

[a] Error was estimated from comparing measures in NaCl 10 mM at different stages of the experiment.

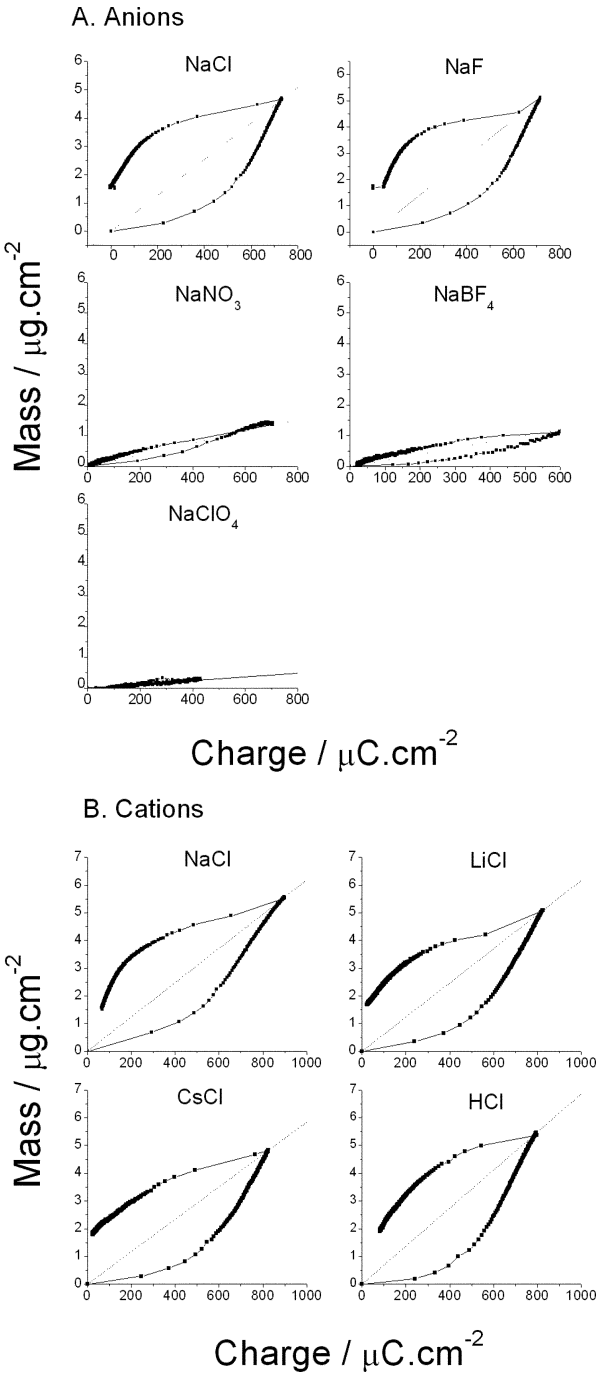

Fig. 5 Mass to charge relationships for data in Fig. 2. Each graph depicts one redox cycle: (1) oxidation at 0.6 V for 60 s (2) reduction at 0.1 V for 60 s. Dotted line slope is end to end exchanged mass (see Table 3).

slow cyclic potential scan in 10 mM NaCl and $NaClO_4$. The general trend is that the film swells during oxidation and shrinks during reduction, as expected from EQCM results. The refractive index, n, decreases upon oxidation as a result of the uptake of water ($n H_2O$: 1.33). The thickness–potential curves also present some hysteresis, which means that even at scan rates as low as 20 mV s^{-1} the flux of solvent is slower than the ionic movement. The origin of the slow solvent flux could

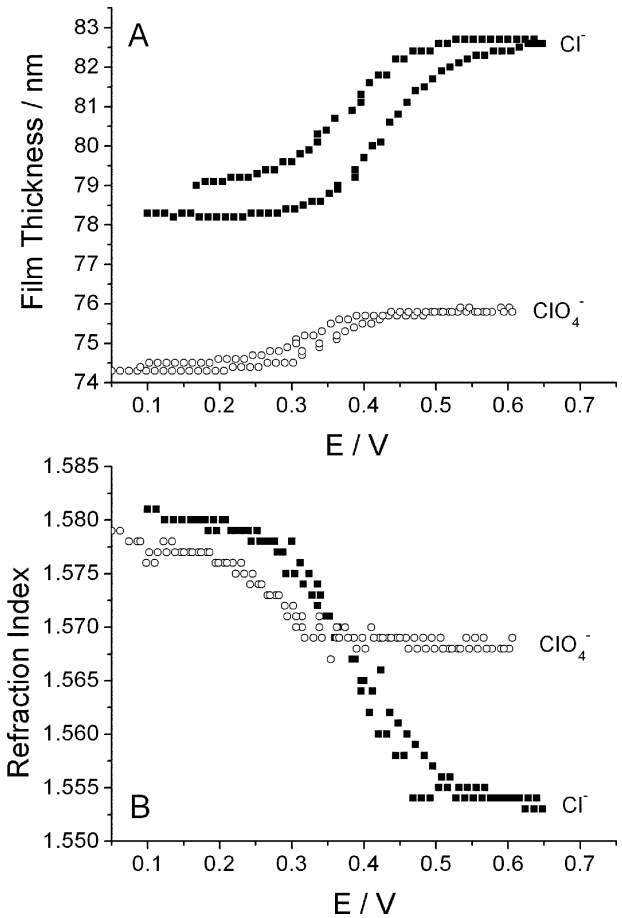

Fig. 6 Film thickness (A) and refractive index at 632.8 nm (B) during potential scan at 20 mV s^{-1} for $(PAH\text{-}Os)_{15}(PSS)_{14}$ film in 10 mM NaCl (black squares) and $NaClO_4$ (open circles).

be related to the slow relaxation of polymer chains to a new structural conformation produced by the change in the redox state of tethered osmium centers.

Although the curves recorded in the presence of both chloride and perchlorate show similar qualitative behavior, there are quantitative differences. The initial film thickness is 5% smaller in $NaClO_4$ solution (the same electrode was used in all measurements). Furthermore, the increase in thickness due to the electrochemical oxidation is 2.6 times larger for NaCl than for $NaClO_4$, which is consistent with EQCM results. The variation in the refractive index is also larger for NaCl than for $NaClO_4$ suggesting that less water molecules enter the film in the latter case.

Fig. 7 shows the film thickness dependence on the fraction of the oxidized osmium sites in the film during the oxidation process (calculated as the ratio of the injected charge to the maximum injected charge). An almost linear dependence on the fraction of oxidized sites can be observed, which suggests that all redox sites which are electrochemically accessible within the experimental timescale, contribute similarly to the redox driven swelling.

Table 4 compiles the ellipsometric film thickness and its variation after oxidation for osmium films in different electrolytes.

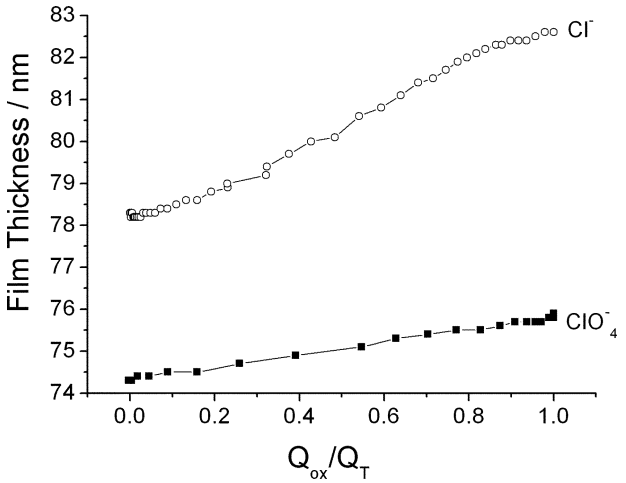

Fig. 7 Film thickness as a function of the fraction of oxidized osmium sites during cyclic voltammetry for a $(PAH\text{-}Os)_{15}(PSS)_{14}$ film in 10 mM NaCl (black squares) and $NaClO_4$ (open circles).

Table 4 Ellipsometric film thickness in reduced state, d_f and change in film thickness upon oxidation Δd_f for potential scan measurements

	HCl	LiCl	NaCl	CsCl	$NaClO_4$
d_f/nm	78.8	76.6	78.2	80.1	74.3
Δd_f/nm	5.9	3.9	4.5	3.6	1.6

3. Disscusion

The results presented in the previous section showed that the electrochemical behavior and the redox driven swelling for PAH-Os/PVS films are strongly influenced by the choice of the anion in the bathing electrolyte. On the the other hand, for the same anion all the cations analyzed produced similar results.

This difference could be explained considering that at the low electrolyte concentrations employed in this work (10 mM) Donnan permselectivity conditions[28] are fulfilled and therefore only anion exchange takes place during redox switching.

At this point it is worthwhile noting the remarkable effect produced by perchlorate in cyclic voltammetry, EI spectra and chronoamperometric transients. The decrease in redox charge, peak separation and tailing in the cyclic voltamperograms and the nonlinear dependence between peak current and scan rate suggests that the transport of electrons within the film is slowed down in the presence of this anion as confirmed by the extremely low electron diffusion coefficient obtained from EIS experiments. An increase in the charge transfer resistance also resulted from EI spectra measured in perchlorate solutions. This may be explained assuming that in our simple equivalent circuit, this resistance accounts not only for the electron charge transfer at the film–metal interface but also for the ohmic resistance of the film.

The effect of perchlorate on the electron transport reported here for the first time for a layer-by-layer self-assembled redox PEM modified electrode, has previously been observed in redox hydrogels. Oh and Faulkner reported this effect of ClO_4^- on voltamperograms for the complex $Ru(bpy)_2Cl^+$ attached to a quaternized poly(4-vinylpyridine) QPVP.[46]

Measurements of ionic conductivity, IR spectroscopy[47] and a luminescent probe[46] have shown that perchlorate anion interacts strongly with QPVP matrix leading to film dehydration. Based on these results these authors suggested that perchlorate anions could ion pair to fixed positive charges in the matrix or to redox groups due to its high hydrophobicity, producing electrostatic cross linking in the film which would affect the segmental mobility of pendant metal complexes decreasing the electron hopping rate. Aoki and Heller[48] also reported a similar behavior in cyclic voltammetry for a redox hydrogel comprised of an ethylamine quaternized poly-(4-vinylpyridine) complex of $Os(bpy)_2Cl^{+/2+}$ and found a decrease in the steady state current for a generator–collector experiment when perchlorate was used in the electrolyte solution.

The theoretical approach of Savéant[49] has shown that when mobile electroinactive ions became ion-paired to immobile electroactive sites, the charge-transport rate presents a sharp decrease as the ion association constant increases if these ion-paired sites are unable to participate in the electron hopping.

Based on the evidence and these ideas, we conclude that the hindrance for the electron transport produced by perchlorate anions in PAH-Os/PVS films is due to the association of perchlorate with charged groups in the film, limiting the mobility of the redox sites.

We will now turn our attention to the redox driven swelling of PAH-Os/PVS films. We have shown that this process is controlled by the nature of the anion. The following conclusions can be drawn by examination of Table 5 which compiles the molar masses, ionic radii both in the crystal and in solution and the hydration numbers for the sudied ions.

1. The exchanged molar mass in all EQCM experiments is much greater for all electrolytes (except for $NaClO_4$) than the molar mass of any of the ions including their coordination water. This means that during oxidation an important amount of neutrals (water and salt) enter the film due to osmotic forces. Under Donnan permselectivity conditions, salt is not exchanged and therefore only solvent can contribute to the molar mass of exchanged neutral species:

$$\Delta M_{\text{neutrals}} = \frac{F\Delta m}{q} - M_{\text{anions}} \qquad (4)$$

where Δm is the exchanged areal mass density, q the charge density passed through the electrode and M_{ions} the molar mass of the counterions.

2. No general trend for the redox swelling dependence on the anion based on molar masses or ionic radii could be identified so that it can be concluded that ion diffusion is not an important limiting condition in the present results.

To gain a further insight in the process under discussion, it is worth analysing the contributions to the osmotic forces during swelling and redox driven swelling of LbL self-assembled PEMs. The swelling behavior of charged polymer networks immersed in an electrolyte solution can be described considering the changes in the total osmotic pressure when the film swells or shrinks. At equilibrium the free energy is at minimum with respect to the film thickness (for a film in mechanical

Table 5 Physical-chemical data for the ions employed in this work compiled from refs. 58 and 59

	Molar mass/g mol^{-1}	Ionic radius/pm	Hydration radius/pm	Hydration number
Anions				
Cl^-	35.45	180	319	6–8
F^-	19.00	263	124	4–6
NO_3^-	62.00	316	177	6
BF_4^-	86.81	—	—	—
ClO_4^-	100	370	241	4–5
Cations				
Na^+	22.99	236	97	6
Cs^+	132.9	314	173	8
Li^+	6.94	208	71	4
H_3O^+	1.008	275	141	4

equilibrium) so that:

$$\Pi = -\frac{\partial G}{\partial V}\Big)_T = -\frac{1}{A}\frac{\partial G}{\partial d}\Big)_T = 0 \qquad (5)$$

where Π is the total osmotic pressure and G is the system free energy. Most authors [50–53] recognize four independent different contributions to the free energy, and hence to the osmotic pressure:

$$\Pi = \Pi_{el} + \Pi_{coul} + \Pi_{mix} + \Pi_{ion} \qquad (6)$$

The elastic contribution of the polymer chains is represented here by $\Pi_{el.}$ This term always carries a negative sign if the unswollen film is taken as the reference state and its origin is purely entropic.[53] The term Π_{coul} accounts for the repulsion between fixed charges in the polymer, which are partially screened by the ions within the gel. The mixing term, Π_{mix}, contains both entropic and enthalpic contributions for the mixing of the polymer backbone and the solvent, and is often calculated with the Flory–Huggins lattice theory.[54]

The last term in eqn (6), Π_{ion} contains the contributions from the translational entropies of ions inside the film:[52]

$$\Pi_{ion} = RT\left(\sum_i c_i - c_i'\right) \qquad (7)$$

where c_i and c_i' are the concentrations of the ith ion within the film and in solution, respectively. For a 1 : 1 electrolyte with c_{salt} concentration and under Donnan permselectivity conditions, the concentration of counterions inside the film is equal to the number of fixed charges, c_{fix}.

Therefore the expression (7) now reads:

$$\Pi_{ion} = RT(c_{fix} - 2c_{salt}) \qquad (8)$$

It is worth mentioning that for ampholytic films (such as LbL multilayers) c_{fix} should be regarded as the difference between the concentration of positive and negative fixed charges in the film.[51] Swelling and electrochemically induced swelling could then be explained qualitatively employing eqns (1) and (2). Consider, for example, the difference in salt induced volume changes of polyelectrolyte gels and LbL multilayers. While the former shrink when the electrolyte concentration increases[50,53] due to a decrease in the osmotic pressure Π_{ion} (the other contributions being constant), multilayer films swell when electrolyte concentration increases[16] since the decrease in the osmotic pressure Π_{ion} is overcome by the network relaxation produced by the break of electrostatic crosslinks by salt, which could be thought as a shift of Π_{el} towards less negative values.

When an anion exchanger film bearing positive net fixed charges is oxidized (reduced), the redox switching creates (destroys) fixed charges within the film. When new charges are created an anion influx should occur to maintain electroneutrality and this increases Π_{ion} due to the increase in the number of ions within the film and also Π_{coul} increases due to an increase in the electrostatic repulsion between the positive fixed charges in the film. As a result, the film swells until a new equilibrium condition is achieved when the osmotic and elastic forces are in balance. Upon film reduction the inverse processes take place.

The dependence of the observed molar masses of exchanged ions on the nature of the anion can be rationalized by assuming that some anions can ion-pair to the newly created osmium (III) sites:

$$\mathrm{Pol-Os(II)^+ \rightarrow Pol-Os(III)^{2+} + e^-} \qquad (9)$$

$$\mathrm{Pol-Os(III)^{+2} + X^- \overset{K'_{eq}}{\rightleftharpoons} \left[Pol-Os(III)^{2+}X^-\right]} \qquad (10)$$

In this case the neutral ion-pair does not contribute to increase Π_{ion} and Π_{coul} and thus to the film swelling. The ion-pairing of the free protonated amino groups of PAH-Os to the anion may also contribute:

$$\mathrm{Pol-NH_3^+ + X^- \overset{K'_{eq}}{\rightleftharpoons} \left[Pol-NH_3^+X^-\right]} \qquad (11)$$

In this respect, Szwarc[55] has distinguished between "solvated ion-pair" and "contact ion-pair". Jeschke *et al.*[56] have demonstrated by electron spin resonance the spatial distribution and dynamics of "contact ion pairs" formed by site binding of divalent anions to soluble cationic poly(diallyldimethylammonium chloride) polyelectrolyte.

The condensation of perchlorate and amino groups in this equilibrium would make Π_{el} more negative due to crosslinking. This contribution to the overall effect is, however, controversial since Schlenoff *et al.*[17,18] have shown for LbL-self-assembled PEMs that the charged groups in polyanions and polycations compensate each other (intrinsic charge compensation), except at the film–solution interface.

The dependence of reduced film thickness with the electrolyte anion (Table 4) can also be explained considering eqn (11), since pairing between free amino groups and perchlorate will reduce Π_{ion} and Π_{coul} leading to film de-swelling.

The smallest exchanged molar mass is observed when using ClO_4^- or BF_4^-. We have shown that ClO_4^-, and to a lesser extend BF_4^-, also produce a significant decrease in the electrochemical response due to a decrease in the electron hopping diffusion coefficient. Therefore these anions should present greatest pairing constant (k_{eq} in eqn (10)). When the supporting electrolyte contains NO_3^- the exchanged molar mass is larger than for ClO_4^- but still less than for Cl^- or F^-. The cyclic voltammetry for PAH-Os/PVS multilayer in this case is

reversible and the current transients integrate to almost the same charge as for Cl^- and F^-; thus we can conclude that some ion pairing would occur for NO_3^-, but is not important enough to modify the charge transport in the time scales employed in this work.

Finally Cl^- and F^- exhibit the largest exchanged mass and the maximum charge, so we conclude that ion pairing is not so important with these anions.

The ability of anions to form ion pairs with osmium sites (and probably with cationic sites of the multilayer in general) decreases in the order: $ClO_4^- \gg BF_4^- > NO_3^- > Cl^-, F^-$. This is in close resemblance with the well known Hofmeister series.

Site binding to these polyelectrolytes by anions that favour contact ion pairing results in hydrophilic to hydrophobic transformation with the collapse of polymer chains into a less solvated state.[57]

4. Conclusions

The charge transport and the electrochemically driven redox swelling have been studied for PAH-Os/PVS films as a function of the composition of the electrolyte, employing cyclic voltammetry, electrochemical impedance spectroscopy, electrochemical quartz crystal microbalance and *in situ* ellipsometry.

At low sweep rate, the voltamperograms show a thin film Nernstian behavior for all electrolytes employed, except for $NaClO_4$ where diffusional behavior could be observed. In the latter case, the hydrophobic ClO_4^- ion pairs with fixed charges in the multilayer, leading to dehydratation and crosslinking. This produces a constraint in the segmental mobility of the osmium sites which drastically reduces the apparent diffusion coefficient for electron transport, as is revealed by EIS.

EQCM and *in situ* ellipsometry have shown that the film mass and thickness (volume) increases during oxidation and decreases during reduction. The observed exchanged masses could only be explained assuming that the water is exchanged in large excess to the counter-ions hydration water. A thermodynamic explanation to this phenomenon has been proposed based on the different contributions to the osmotic pressure.

Mass to charge plots also reveal that solvent fluxes are always slower than charge injection in the multilayer film. It is suggested that the uptake of solvent needs slow polymer chain relaxation to create a cavity within the film.

The amount of exchanged water is very dependent on the anion in the electrolyte but not on the cation as expected for an anion exchanger film. The smaller exchanged masses observed for NO_3^-, BF_4^- and ClO_4^- could not simply be explained as a consequence of a decrease in the injected charge. The final hydration of the film should therefore depend on the anion employed and on its ability to ion-pair with fixed redox and non redox charged sites in the film, even in the case where the charge transport is not directly affected.

As a conclusion, we have demonstrated that the electrochemistry of PEM redox multilayers is highly dependent on the electrolyte employed and therefore its correct choice is crucial for any application based on redox PEM modified electrodes.

Acknowledgements

The authors are grateful to CONICET, University of Buenos Aires and ANPCyT for financial support. M.T. acknowledges a cooperative research doctoral fellowship from CONICET and TENARIS Corp.

References

1 S. S. Shiratori and M. F. Rubner, *Macromolecules*, 2000, **33**, 4213–4219.
2 G. Decher, in *Multilayer Thin Films*, ed. G. Decher and B. J. Schlenoff, Wiley-VCH, Weinheim, Editon edn, 2003.
3 X. Arys, A. M. Jonas, A. Laschewsky and R. Legras, in *Supramolecular Polymers*, ed. A. Ciferri, Marcel Dekker, New York, Editon edn, 2000.
4 A. Fery, B. Schöler, T. Cassagneau and F. Caruso, *Langmuir*, 2001, **17**, 8779–8783.
5 D. E. Grumelli, A. Wolosiuk, E. Forzani, G. A. Planes, C. Barbero and E. J. Calvo, *Chem. Commun*., 2003, 3014–3015.
6 M. Tagliazucchi and E. J. Calvo, *J. Electroanal. Chem*., 2006, in press.
7 D. Laurent and J. B. Schlenoff, *Langmuir*, 1997, **13**, 1552–1557.
8 J. Stepp and J. B. Schlenoff, *J. Electrochem. Soc*., 1997, **144**, 155–157.
9 R. J. E. Hodak, E. J. Calvo, K. Singhal and P. N. Bartlett, *Langmuir*, 1997, **13**, 2708–2716.
10 V. Flexer, E. S. Forzani, S. Ludueña, L. Pietrasanta and E. J. Calvo, *Anal. Chem*., 2005.
11 E. S. Forzani, M. Otero, M. A. Perez, M. L. Teijelo and E. J. Calvo, *Langmuir*, 2002, **18**, 4020–4029.
12 E. S. Forzani, M. A. Perez, M. L. Teijelo and E. J. Calvo, *Langmuir*, 2002, **18**, 9867–9873.
13 L. Cheng, L. Niu, J. Gong and S. Dong, *Chem. Mater*., 1999, **11**, 1465–1475.
14 M. K. Beissenhirtz, F. W. Scheller and F. Lisdat, *Anal. Chem*., 2004, **76**, 4665–4671.
15 J. W. Baur, S. Kim, P. B. Balanda, J. R. Reynolds and M. F. Rubner, *Adv. Mater*., 1998, **10**, 1452–1455.
16 S. T. Dubas and J. B. Schlenoff, *Langmuir*, 2001, **17**, 7725–7727.
17 T. R. Farhat and J. B. Schlenoff, *Langmuir*, 2001, **17**, 1184–1192.
18 T. R. Farhat and J. B. Schlenoff, *J. Am. Chem. Soc*., 2003, **125**, 4627–4636.
19 H. W. Jomma and J. B. Schlenoff, *Macromolecules*, 2005, **38**, 8473–8480.
20 K. Itano, J. Choi and M. Rubner, *Macromolecules*, 2005, **38**, 3450–3460.
21 L. Zhai, A. J. Nolte, R. E. Cohen and M. Rubner, *Macromolecules*, 2004, **37**, 6113–6123.
22 R. M. Torresi, S. I. C. d. Torresi, C. Gabrielli, M. Keddam and H. Takenoutti, *Synth. Met*., 1993, **61**, 291–296.
23 C. Barbero, M. C. Miras, O. Haas and R. Kötz, *J. Electrochem. Soc*., 1997, **144**, 4170–4174.
24 C. Barbero, M. C. Miras, E. J. Calvo, R. Kötz and O. Haas, *Langmuir*, 2002, **18**, 2756–2764.
25 I. Jureviciute, S. Bruckenstein and A. R. Hillman, *Electrochim. Acta*, 2006, **51**, 2351–2357.
26 I. Jureviciute, S. Bruckenstein and A. R. Hillman, *J. Electroanal. Chem*., 2000, **488**, 73–81.
27 M. Tagliazucchi, D. Grumelli, C. Bonazzola and E. J. Calvo, *J. Nanosci. Nanotechnol*., 2006, **6**, 1731–1740.
28 E. J. Calvo and A. Wolosiuk, *J. Am. Chem. Soc*., 2002, **124**, 8490–8497.
29 D. Grumelli, F. Garay, C. Barbero and E. Calvo, *J. Phys. Chem. B*, 2006, in press.
30 C. Danilowicz, E. Corton and F. Battaglini, *J. Electroanal. Chem*., 1998, **445**, 89.
31 J. Choi and M. F. Rubner, *Macromolecules*, 2005, **38**, 116–124.
32 J. Hodak, R. Etchenique, K. Singhal, P. N. Bartlett and E. J. Calvo, *Langmuir*, 1997, **13**, 2708–2716.
33 H. O. Finklea, D. A. Snider and J. Fedyk, *Langmuir*, 1990, **6**, 371.
34 E. Calvo, C. Danilowicz and R. Etchenique, *J. Chem. Soc., Faraday Trans*., 1995, **91**, 4083.

35 E. J. Calvo, E. Forzani and M. Otero, *J. Electroanal. Chem.*, 2002, **538/539**, 231–241.
36 E. J. Calvo, E. S. Forzani and M. Otero, *J. Electroanal. Chem.*, 2002, **231**, 538.
37 E. Laviron, *J. Electroanal. Chem.*, 1979, **101**, 19–28.
38 E. Laviron, L. Roullier and C. Degrand, *J. Electroanal. Chem.*, 1980, **112**, 11–23.
39 M. Tagliazucchi and E. J. Calvo, 2006, in preparation.
40 A. J. Bard and L. R. Faulkner, *Electrochem. Meth.*, John Wiley and Sons, 2001.
41 J. E. B. Randles, *Discuss. Faraday Soc.*, 1947, **1**, 11.
42 C. Gabrielli, O. Haas and H. Takenouti, *J. Appl. Electrochem.*, 1987, **17**, 82–90.
43 G. J. Brug, A. L. G. V. D. Eeden, M. Sluyters-Rehbach and J. H. Sluyters, *J. Electroanal. Chem*, 1984, **176**, 275–295.
44 A. R. Hillman, *Solid State Ionics*, 1997, **94**, 151–160.
45 I. Jureviciute, S. Bruckenstein, A. R. Hillman and A. Jackson, *Phys. Chem. Chem. Phys.*, 2000, **2**.
46 S. M. Oh and L. R. Faulkner, *J. Am. Chem. Soc.*, 1989, **111**, 5613–5618.
47 S. M. Oh and L. R. Faulkner, *J. Electroanal. Chem.*, 1989, **269**, 77–97.
48 A. Aoki and A. Heller, *J. Phys. Chem.*, 1993, **97**, 11014–11019.
49 J. M. Savéant, *J. Phys. Chem.*, 1988, **92**, 4526–4532.
50 T. Barenbrug, D. Bedeaux and S. J. A. M., *Macromolecules*, 1999, **32**, 199–209.
51 A. E. English, S. Mafé, J. A. Manzanares, X. Yu, A. Y. Grosberg and T. Tanaka, *J. Chem. Phys.*, 1996, **104**, 8713–8720.
52 J. Ricka and T. Tanaka, *Macromolecules*, 1984, **17**, 2916–2921.
53 T. L. Hill, *An Introduction to Statistical Thermodynamics*, Dover Publications, New York, 1986.
54 P. J. Flory, *Principles of Polymer Chemistry*, Cornell University Press, Ithaca, New York, 1953.
55 M. Szwarc, *Acc. Chem. Res.*, 1969, **2**, 87–96.
56 D. Hinderberger, H. W. Spiess and G. Jeschke, *J. Phys. Chem. B*, 2004, **108**, 3698–3704.
57 O. Azzaroni, S. Montoya, T. Farhan, A. A. Brown and W. T. S. Huck, *Macromolecules*, 2005, **38**, 10192–10199.
58 H. Ohtaki and T. Radnai, *Chem. Rev.*, 1993, **93**, 1157.
59 Y. Marcus, *Chem. Rev.*, 1988, **88**, 1475.